GPS Solutions (2020) 24:5
https://doi.org/10.1007/s10291-019-0917-0

ORIGINAL ARTICLE

A model for assessing the impact of linear and nonlinear distortions on a GNSS receiver

Mariano Vergara[1,3] · Felix Antreich[2,4] · Christoph Enneking[2] · Matteo Sgammini[2] · Gonzalo Seco-Granados[3]

Received: 7 March 2018 / Accepted: 10 October 2019

Abstract
The tracking performance of a global navigation satellite system (GNSS) receiver is altered by signal distortions of different kinds, ranging from transmitter and receiver imperfections to various forms of channel impairments. Accurate modeling of the receiver performance in the presence of signal distortions allows to improve GNSS-based positioning, tighten error bounds, and thus enhance the integrity and the availability of the GNSS services. We present a model for the code-tracking loop performance of a GNSS receiver when the GNSS signal undergoes an arbitrary cascade of nonlinear and linear distortions. The impact of the distortions on the pseudorange estimation is analyzed by deriving closed-form expressions for the bias and variance of the tracking error. These analytical expressions are based on the well-known open-loop linearized delay-locked loop model. The validation is then performed using a GNSS software receiver that evaluates the tracking error numerically.

Keywords Signal quality monitoring · Evil waveforms · Tracking performance · Delay-locked loop (DLL)

Introduction

New types of safety–critical global navigation satellite systems (GNSSs) applications impose significant requirements on the quality of GNSS signals. Signals radiated by satellites can be affected by imperfections and faulty satellite hardware, thus making the signal models used in the signal-in-space interface control documents (SIS ICD) less representative of the actual signal processed at the receiver side. Certain GNSS services, for example safety-of-life (SoL) services, have very stringent requirements, and they are particularly sensitive to degradation of the GNSS signal quality. When the GNSS signal becomes more disturbed, the position accuracy is likely to deteriorate, and the bounds on the ranging error become less reliable, thus jeopardizing system integrity. Furthermore, satellite signal distortions may affect the users in different ways depending on several receiver parameters such as receiver bandwidth, correlator spacing, discriminator type and tracking loop. An accurate characterization of the error induced by signal deformation is then required in order to ensure the integrity of the service.

The causes and the types of these distortions are manifold: high-power amplifier distortions, frequency selectivity of the transmission medium, satellite inherent multipath and the effect of the receiver front-end filtering contributing to degrading the GNSS signals available for processing at the receiver. Such imperfections can be observed on a multitude of GNSS satellites (Phelts and Akos 2006). Some of these signal imperfections can be considered acceptable, and the label of nominal signal distortions is often used in the literature (Van Dierendonck et al. 2000a, b). Other signal imperfections lie beyond certain service-dependent acceptability thresholds, as it is likely to happen in the presence of a satellite hardware fault. These anomalous signal distortions are also known as evil waveforms (Phelts 2001). There is no broad consensus yet on how the threshold between nominal signal distortions and anomalous signal distortions ought to be determined, the main problem being the lack of agreement on the choice of a proper metric with which to appraise the gravity of the signal degradation.

The International Civil Aviation Organization (ICAO) defines two models for a linear and a nonlinear distortion

✉ Mariano Vergara
mariano.vergara@airbus.com

1 Airbus Defense and Space GmbH, Taufkirchen, Germany

2 German Aerospace Center (DLR), Wessling, Germany

3 IEEC-CERES, Universitat Autònoma de Barcelona (UAB), Barcelona, Spain

4 Aeronautics Institute of Technology (ITA), São José dos Campos, Brazil

Published online: 07 November 2019

(ICAO 2001). The model for the linear distortion called threat model B, also known as analog distortion, consists in a second-order step response. Threat model A, also known as digital distortion, is a nonlinear distortion in which the falling edges of a binary modulated signal are either delayed or advanced. The ICAO also defines a threat model C, which is the superposition of threat model A and threat model B.

One of the difficulties regarding the GNSS signal distortion problem is that the impact of such a threat on users depends upon two fundamental parameters: the signal modulation and the GNSS receiver processing. For this reason, the recommendations as given in ICAO (2001) for the nominal ranges of the parameters describing threat model A and threat model B distortions can only be indicative. If a GNSS service and a receiver configuration are given, it is possible to produce a more accurate limit between nominal and non-nominal distortions. Particularly, problematic is then the assessment of the receiver performance in the presence of the threat model C, as the linear (threat model B) and nonlinear (threat model A) distortion has a joint nonlinear effect on the receiver performance.

Several works on the topic of GNSS signal quality monitoring (SQM) have further investigated these ICAO guidelines. In Phelts et al. (2009), the effects on GNSS signals of the ICAO threat model B are analyzed regarding step responses, frequency responses and group delay when the threat model B lies within the nominal parameter ranges defined in ICAO (2001). In Wong et al. (2011), it is observed that step response is not always an accurate measure of the deterioration of the positioning solution experienced by the GNSS user. Furthermore, evidence suggests that the second-order system model for the linear (analog) distortions proposed in ICAO (2001) might not be appropriate for all GNSS signals and frequencies and all satellites under observation. For example, the second-order ICAO model seems to be acceptable for signals with high time-bandwidth products, i.e., signals with few spectral side lobes in the useful bandwidth, but this model is not appropriate for signals with lower time-bandwidth products (Vergara et al. 2016).

Threat model A, or digital distortion, is a type of signal distortion particularly critical for fine signal synchronization, and it received attention from the civil aviation community already in early times (Van Dierendonck et al. 2000a, b; Akos et al. 2000). In Mittelman et al. (2004), the digital distortion is estimated for all 24 GPS satellites. In Phelts and Akos (2006), deformations of the cross-correlation function due to the digital distortions are studied for modernized GNSS signals and the dependency on the receiver correlator spacing is highlighted. In Hegarty and Van Dierendonck (2008), a model for the impact of the digital distortion on the tracking error is proposed, though the analysis is restricted to non-band-limited signals and no model for a GNSS receiver is considered. Previous publications on the topic leave open the problem of how to assess the GNSS receiver performance in the ICAO threat model C case. Indeed, the degradation of the tracking performance caused by the digital distortion cannot merely be added to the degradation caused by the linear distortion, as these effects are interdependent, and sometimes they add up constructively, and sometimes they compensate each other, depending on several factors including the GNSS receiver structure. Outside the GNSS community, the digital distortion has been studied by Bishop et al. (1998) and Simon and Million (1996).

Other contributions focused on other types of distortions not included in the ICAO threat models. For example, in Soellner et al. (2002) several signal distortions are contemplated: sinusoidal amplitude ripple, linear amplitude slope, phase distortions and spurious emissions due to high-power amplifiers (HPA). The impact of these distortions on the GNSS receiver performance is assessed regarding correlation loss, S-curve slope and tracking error bias. These assessments are based on computer simulations. The impact of the signal distortions on the change in the S-curve slope is also mentioned. The analysis of this latter phenomenon can be included in the calculation of the variance of the tracking error, enabling a more accurate error performance model (Vergara et al. 2009), and hence tighter error bounds.

A possible way to quantify the impact of signal distortions on a GNSS system is to include the signal distortions in the calculations of the tracking performance of the GNSS receiver. A result of this kind would allow us to predict, bound and mitigate the error in the pseudorange measurements, enhancing GNSS integrity and positioning accuracy. The tracking performance of a GNSS receiver can be categorized as either in dynamic or steady state. The dynamic tracking performance includes transient pull-in and loss of lock performance. The steady-state performance characterizes the tracking error of the GNSS receiver, when time-dependent factors are either not dominant or not present at all.

In this work, we focus exclusively on the steady-state performance analysis. The steady-state performance of a GNSS receiver is adequately described by a stochastic characterization of the tracking error. In Wu et al. (2002), the reader can find a comprehensive description of the delay-locked loop (DLL) functioning and its linearized model, which is used for the steady-state performance analysis. In Holmes (2007), the steady-state performance of a DLL is presented for several DLL architectures.

The tracking error bias, in particular, the one that is caused by multipath propagation, has been investigated by several authors (Braasch 1992; Van Nee 1995; Irsigler 2008). Most of these results assume ideal non-band-limited signals and are concerned with the bounding of the tracking error bias (e.g., multipath error envelope), rather than calculating it. Moreover, their focus is restricted to the tracking

error bias arising from two-path propagation models. Multipath propagation can be seen as a particular form of linear distortion, and our model is valid also for the study cases considered in the references above. The impact of receiver front-end filtering on the tracking accuracy of a GNSS receiver was treated in Holmes (1997). Betz and Kolodziejski (2009) studied the variance of the tracking error in case of non-white interference and arbitrary band-limited signal pulse shapes, assuming that the interference and the noise do not induce a bias in the tracking error, and thus, the tracking error was characterized only in terms of variance.

With the tools presented in this work, we propose an analytical approach to assess the severity of the effect of GNSS signal deformations on the receiver performance and thus pave the way for the definition of new service-dependent signal quality requirements. The proposed model contemplates a cascade of arbitrary nonlinear and linear distortions. The receiver performance is quantified using the bias and variance of the tracking error. As in Betz and Kolodziejski (2009), the analysis is carried out for an arbitrary chip pulse shape. The linear distortion accounts for effects such as multipath propagation and linear filtering due to satellite payload imperfections or the receiver front end. The nonlinear distortion accounts for a variety of nonlinear effects experienced by the ranging signal before the linear distortion. One of the elements of the novelty of the work is that the proposed performance model holds for any linear and nonlinear distortion. Our proposed performance model requires the nonlinear distortion to be described either in terms of a parameterization of the cross-correlation between the ideal ranging signal and its distorted version or by an empirical model of the latter. The distorted cross-correlation can also be characterized in the frequency domain, under the form of a cross-power spectrum (CPS). The model that we present here allows us to calculate also performance metrics as the differential tracking error without the need for time-consuming computer simulations; the latter are needed in Pagot et al. (2016), for example.

After having introduced the notation and the signal distortion model, we delineate the assumptions made on the receiver, which is based on a closed-loop implementation of a maximum-likelihood estimator for the time delay. Next, we describe the effect of the signal distortions in the receiver processing, and then, we derive the analytical formulas for the bias and the variance of the tracking error. Lastly, we present a study case in which the nonlinear distortion under investigation is based on the ICAO threat model A. For this case, we compare the results obtained by particularizing the analytical formulas for the case of a DS-CDMA signal with two different pulse shapes: a rectangular pulse shape and a binary offset carrier (BOC) pulse shape. The results obtained through analytical calculations are validated by computer simulations made with a software GNSS receiver.

Signal distortion model

The signal received by the GNSS receiver is modeled as the noisy output of a time-invariant system consisting of a cascade of a nonlinear transformation and a linear transformation, as depicted in Fig. 1. The nonlinear transformation is indicated by T[·], and the linear transformation is described by the convolution of the impulse responses $h_{Tx}(t)$ and $h_{Rx}(t)$, which account for the linear distortions due to the transmitter payload and the receiver front end, respectively. Let the nominal ideal signal be $c(t)$, which is input to the cascade in Fig. 1. After the receiver front end, the baseband signal can be expressed as

$$r(t) = \sqrt{P}\mathrm{T}[c(t)] \otimes h_{Tx}(t) \otimes h_{Rx}(t) + n_{Rx}(t) \tag{1}$$

where symbol $\otimes$ indicates the convolution operation. Let $s(t) = \sqrt{P}\mathrm{T}[c(t)] \otimes h_{Tx}(t) \otimes h_{Rx}(t)$ and $h(t) = h_{Tx}(t) \otimes h_{Rx}(t)$. The noise term after the receiver front-end filtering is indicated by

$$n_{Rx}(t) = n(t) \otimes h_{Rx}(t) \tag{2}$$

with $n(t)$ being proper complex Gaussian noise with power spectral density of N_0. In proper complex Gaussian noise, the real and imaginary parts are uncorrelated. In the following, we shall assume that $h_{Rx}(t)$ is a Dirac Delta, so sampling $h(t)$ yields still additive white Gaussian noise (AWGN). If this were not the case, i.e., for an arbitrary $h_{Rx}(t)$, the results presented here would hold only partially. Formulas for the tracking error bias would still be valid since this quantity is not impacted by the noise variance. If $h_{Rx}(t)$ were arbitrary, noise at correlator output would not be AWGN anymore, and the formulas for the tracking error variance derived in this analysis would be inaccurate. We note, however, that it is a common practice in the literature to perform integrity analyses based only on the pseudorange biases, assuming that a satellite fault does not change the variance of the pseudorange error, see, e.g., Soualle et al. (2015), Zaugg (2002) and Van Dierendonck et al. (2000a, b). As a consequence of that, the assumption of Dirac Delta for $h_{Rx}(t)$ does not significantly restrict the applicability of the presented result and yet paves the way for more complete analyses that take

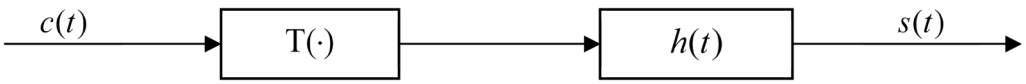

Fig. 1 Distortion model

into account the difference in pseudorange error variances between fault-free and faulty cases.

Let the nominal ranging signal $c(t)$ be a complex signal consisting of a train of pulses:

$$s(t) = \sum_{k=-\infty}^{\infty} a_k g\left(t - kT_c\right) \tag{3}$$

with a_k being the kth symbol, $g(t)$ being the chip pulse shape and T_c being the inverse of the symbol rate, i.e., $T_c = \frac{1}{B_c}$.

Signal (3) can be, for example, direct sequence code division multiple access (DS-CDMA), with a_k the elements of the spreading code. The cascade of the transmitter and receiver impulse response yields the overall impulse response

$$h(t) = h_{Tx}(t) \otimes h_{Rx}(t) \Leftrightarrow H(f) = H_{Tx}(f)H_{Rx}(f) \tag{4}$$

where the symbol $\Leftrightarrow$ is used to express the Fourier transformation. Let the impulse response $h(t)$ have unitary energy so that the output of the nonlinear transformation, T[·], has unitary power:

$$\int_{-\infty}^{\infty} |h(t)|^2 \mathrm{d}t = 1 \tag{5}$$

$$\lim_{U\to\infty} \frac{1}{2U} \int_{-U}^{U} |\mathrm{T}[c(t)]|^2 \mathrm{d}t = 1 \tag{6}$$

As a consequence of these normalizations, the useful signal available for processing at receiver side $s(t)$ has power equal to P.

Receiver model

The tracking performance of the receiver is modeled based on Vergara et al. (2009), where the following assumptions are made:

- *Steady-state tracking* The DLL is already tracking, and the joint effect of distortions plus noise does not cause a loss of lock.
- *Small tracking jitter* The tracking point oscillates around the lock point in a relatively small range of values, for which the composite discriminator is approximately linear. In other words, the tracking error $\varepsilon = \tau - \hat{\tau}$ is small enough to experience a linear discriminator.

The noise at correlator output is Gaussian discrete-time noise. Provided that the signal bandwidth is much larger than the integration time T_p, the noise at the correlator output is also white. The above assumptions allow linearization of the DLL and to derive an analytical model of the tracking performance (Holmes 2007; Wu et al. 2002). In Fig. 2, an early–late DLL block diagram is depicted. The quantities appearing in the figure are the following: Δ indicates the one-sided correlator spacing; B_L is the one-sided closed-loop bandwidth; and LPF indicates the low-pass loop filter, while $e[k]$, $S(\varepsilon;k)$ and $n_T[k]$ indicate the error signal, the value of the discriminator function and the noise term of the error signal at the kth integration or code epoch, respectively. The error signal is low-pass filtered and used to drive the numerically controlled oscillator (NCO) and the code generator that adjust the estimate $\hat{\tau}$ of the true code phase τ. We consider two kinds of DLL: coherent and non-coherent DLL (early–late). In Table 1, the discriminators of these two DLLs are expressed in terms of the normalized cross-correlation function $R_{s\hat{c}}(\varepsilon)$.

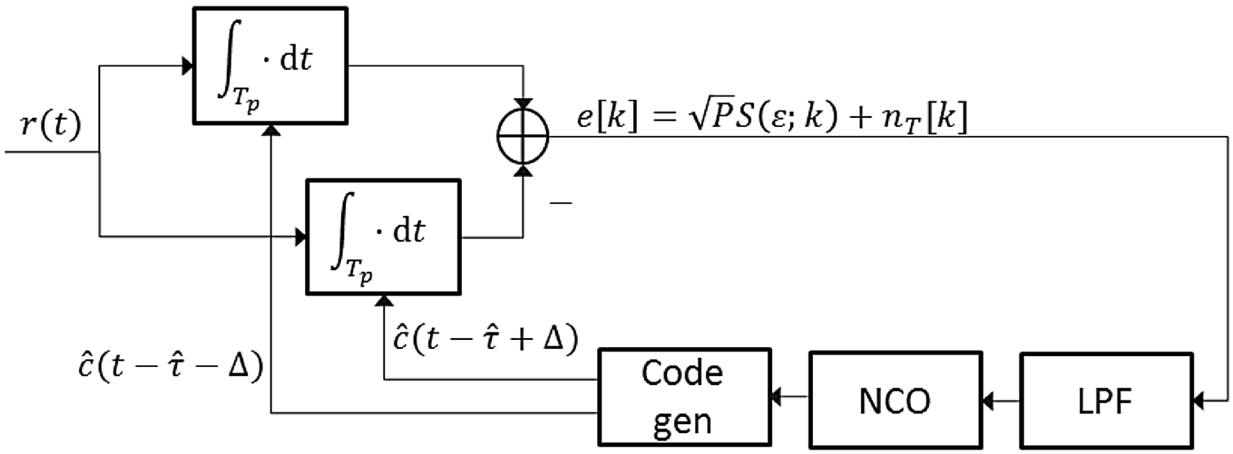

Fig. 2 Delay-locked loop (DLL)

Table 1 DLL discriminators

DLL type	Discriminator
Coherent DLL	$S(\varepsilon) = \mathrm{Re}\{R_{s\hat{c}}(\varepsilon - \Delta)e^{-j\vartheta_c(\varepsilon)}\} - \mathrm{Re}\{R_{s\hat{c}}(\varepsilon + \Delta)e^{-j\vartheta_c(\varepsilon)}\}$
Non-coherent DLL	$S(\varepsilon) = \lvert R_{s\hat{c}}(\varepsilon - \Delta)\rvert^2 - \lvert R_{s\hat{c}}(\varepsilon + \Delta)\rvert^2$

The quantity $\vartheta_c(\varepsilon)$, also given in Table I, is sometimes referred to as a *composite phase*. The composite phase is the phase error that an ideal phase-locked loop (PLL) will inevitably estimate due to eventual power spills from the in-phase (I) component to the quadrature (Q) component. This is likely to happen also in the case of a real ranging, because of the analog distortion or multipath propagation. The composite phase is defined as

$$\vartheta_c(\varepsilon) = \arctan\left(\frac{R^Q_{s\hat{c}}(\varepsilon)}{R^I_{s\hat{c}}(\varepsilon)}\right) \tag{7}$$

where $R^I_{s\hat{c}}(\varepsilon)$ and $R^Q_{s\hat{c}}(\varepsilon)$ are the real (in-phase) and imaginary (quadrature) parts of the cross-correlation function.

Receiver processing

Let $G(f)$ be the Fourier transform of the chip pulse shape $g(t)$ and let the local replica generated by the receiver use another chip pulse shape, not necessarily equal to $g(t)$, to despread the signal. We consider this more general case because employing a non-matched filter can be sensible in situations in which other metrics might have priority over the maximization of the signal-to-noise ratio (SNR). For example, this is the case when new ranging signals are introduced and the maximization of the performance of the new signals is constrained by backward compatibility issues. The local replica generated by the receiver is

$$\hat{c}(t) = \sum_{k=-\infty}^{\infty} a_k \hat{g}\left(t - kT_c\right) \Leftrightarrow \hat{C}(f) \tag{8}$$

with $\hat{g}(t)$ being the chip pulse shape of the replica. Let (8) be a unitary power signal and let its power spectral density (PSD) be denoted by $\boldsymbol{\Phi}_{\hat{c}\hat{c}}(f)$. It then results in

$$\int_{-\infty}^{\infty} \boldsymbol{\Phi}_{\hat{c}\hat{c}}(f)\mathrm{d}f = R_{\hat{c}\hat{c}}(0) = 1 \tag{9}$$

where $R_{\hat{c}\hat{c}}(\tau)$ is the autocorrelation function of $\hat{c}(t)$.

We aim to assess the ranging performance of a delay-locked loop (DLL) receiver that is tracking the signal $s(t)$ in (1). As it is known, the ranging capability of a signal, i.e., the Cramer–Rao lower bound for time-delay estimation, is determined by the PSD of the ranging signal, and in particular by its mean square bandwidth (Kay 1998, Section 3.11). The PSD of a linearly modulated signal is equal to the Fourier transform of the autocorrelation of the pulse shape (Simon et al. 1995, section 3.4), provided that the symbol sequence a_k is infinitely long, zero-mean and with an ideal autocorrelation function. Similarly, if the transmitter and receiver pulse shapes are different, the time-delay estimation performance is determined by the cross-power spectral density (CPS) between the transmitted signal and the locally generated replica. Unfortunately, when the incoming signal undergoes a nonlinear distortion, the CPS cannot always be factorized in the cross-correlation between the symbol sequences and the transmitter and receiver pulse shapes as in Simon et al. (1995, section 3.4). In other terms, the signal $s(t)$ in (1) is not always expressible as a linear combination of a nonlinearly distorted pulse. We can nonetheless continue with our analysis by noting that for the fine synchronization process only the main lobe of the cross-correlation between the incoming distorted signal and the ideal replica is determinant. The performance outside the main lobe of the cross-correlation function has little interest, as the DLL is practically out of lock in this region. The Fourier transform of the cross-correlation between the distorted signal and the ideal local replica, truncated around its main peak, provides all the information necessary for determining the steady-state tracking performance. We refer to this quantity simply as CPS, because from the time-delay estimation problem, it is equivalent to the CPS, despite being only the Fourier transform of a truncated cross-correlation, and not the Fourier transform of the entire cross-correlation, according to the Wiener–Khinchin theorem.

The cross-correlation between the distorted signal and the ideal local replica, given as a function of the tracking error ε, is

$$\begin{aligned} R_{s\hat{c}}(\varepsilon) &= \int_{-\infty}^{\infty} s(t)\hat{c}^*(t+\varepsilon)\mathrm{d}t = (\mathrm{T}[c(t)] \otimes h(t) \otimes \hat{c}^*(-t))(\varepsilon) \\ &= (\mathrm{T}[c(t)] \otimes \hat{c}^*(-t) \otimes h(\tau))(\varepsilon) \end{aligned} \tag{10}$$

where the symbol $()^*$ indicates the operation of the complex conjugate. This expression results directly from the model depicted in Fig. 1, as $\mathrm{T}[c(t)]$ indicates the output of the nonlinear distortion, and $\mathrm{T}[c(t)] \otimes h(t)$ is the output of the linear and nonlinear distortions. Using the associative and commutative properties of the convolution, it is possible to factorize the cross-correlation (10) in two terms:

- a first convolution, denoted by $\varphi(\tau)$, consisting of the cross-correlation between the signal affected by nonlin-

ear distortion and the local replica, in an interval of a chip duration around its main peak:

$$\varphi(\tau) = \int_{-\infty}^{\infty} \mathrm{T}[c(t)]\hat{c}^*(t-\tau)\mathrm{d}t, \quad |\tau| < T_c \tag{11}$$

- a second convolution between $\varphi(\tau)$ and the impulse response $h(\tau)$ describing the linear distortion.

The two convolution factors in (10) can be conveniently expressed in the frequency domain

$$\tilde{R}_{s\hat{c}}(\varepsilon) = \int_{-\infty}^{\infty} \tilde{\Psi}(f) e^{j2\pi f\varepsilon}\mathrm{d}f \tag{12}$$

with

$$\begin{aligned} \tilde{\Psi}(f) &= \Psi_{\mathrm{T}\hat{c}}(f)H(f) \\ \Psi_{\mathrm{T}\hat{c}}(f) &= \int_{-\infty}^{\infty} \varphi(\tau) e^{-j2\pi f\nu}\mathrm{d}\nu \end{aligned} \tag{13}$$

Moreover, let us indicate by $\Phi_{\mathrm{TT}}(f)$ the PSD of the nonlinear distorted signal $\mathrm{T}[c(t)]$. As a consequence of (6), it follows that

$$\int_{-\infty}^{\infty} \Phi_{\mathrm{TT}}(f)df = 1 \tag{14}$$

Therefore, the normalized CPS takes the form

$$\Psi(f) = \frac{\tilde{\Psi}(f)}{\sqrt{\int_{-\infty}^{\infty} \Phi_{TT}(f)|H(f)|^2\mathrm{d}f}} \tag{15}$$

With such a normalization, the main peak of the cross-correlation between the received signal and the local reference has a magnitude of less or equal than one, and it is equal to one exclusively when there are no distortions, and the receiver employs a perfectly matched filter, i.e., $g(t) = \hat{g}(t)$. The CPS given in (15) contains all the information necessary for assessing the performance of a maximum-likelihood time-delay estimator.

The CPS given in (15) in general is complex and, like its time-domain counterpart, does not possess any symmetry. For the calculations presented in the Appendix it is useful to decompose the CPS given in (15) as

$$\Psi(f) = \Psi^R(f) + j\Psi^I(f) = \Psi^R_{\mathrm{even}}(f) + \Psi^R_{\mathrm{odd}}(f) + j\left(\Psi^I_{\mathrm{even}}(f) + \Psi^I_{\mathrm{odd}}(f)\right) \tag{16}$$

with

$$\begin{aligned} \Psi^R_{\mathrm{even}}(f) &= \frac{\Psi^R(f) + \Psi^R(-f)}{2} \\ \Psi^R_{\mathrm{odd}}(f) &= \frac{\Psi^R(f) - \Psi^R(-f)}{2} \\ \Psi^I_{\mathrm{even}}(f) &= \frac{\Psi^I(f) + \Psi^I(-f)}{2} \\ \Psi^I_{\mathrm{odd}}(f) &= \frac{\Psi^I(f) - \Psi^I(-f)}{2} \end{aligned}$$

The normalized cross-correlation can be thus decomposed as

$$\begin{aligned} R_{s\hat{c}}(\varepsilon) &= \int_{-B}^{B} \Psi(f) e^{j2\pi f\varepsilon}\mathrm{d}f \\ &= \int_{-B}^{B} \Psi^R_{\mathrm{even}}(f)\cos(2\pi f\varepsilon)\mathrm{d}f - \int_{-B}^{B} \Psi^I_{odd}(f)\sin(2\pi f\varepsilon)\mathrm{d}f \\ &\quad + j\left[\int_{-B}^{B} \Psi^R_{\mathrm{odd}}(f)\sin(2\pi f\varepsilon)\mathrm{d}f - \int_{-B}^{B} \Psi^I_{\mathrm{even}}(f)\cos(2\pi f\varepsilon)\mathrm{d}f\right] \end{aligned} \tag{17}$$

When no distortions are present, and the receiver uses a local replica matched to the received signal, then only the term $\Psi^R_{\mathrm{even}}(f)$ is present, since the CPS at hand is actually a PSD of a real signal, i.e., a real and even function. The imaginary components of the CPS arise when the cross-correlation function is not symmetric anymore, either because of distortion or because the receiver filter is not matched to the chip pulse shape of the incoming signal.

Tracking performance metrics

The tracking error is a discrete-time random process that at each integration period or code epoch quantifies the time-delay estimation error. We shall provide a statistical characterization of this error in terms of its bias and variance. These quantities fully describe the tracking performance of a GNSS receiver.

Tracking error bias

The bias of the tracking error is the mean of the tracking error, and it is given by the stable tracking point of the DLL which is closest to the initialization point. The initialization point is the timing obtained in the coarse synchronization (acquisition). For a code-tracking loop, a stable tracking point is any zero crossing of the actual discriminator, with a slope that has the same sign as the nominal discriminator

around nominal zero crossing, which is at $\varepsilon = 0$. In our definition (Table 1), the slope of the nominal discriminator, also known as discriminator gain, is positive. For an early–late (and also for a late–early) DLL, the zero crossing of the discriminator represents the value of the code phase for which the early and late correlator output is equal. In nominal conditions, i.e., for the ideal cross-correlation function (17), this necessarily entails that the true code phase τ and its estimate $\hat{\tau}$ coincide, and thus, the tracking error ε is zero. Due to the thermal noise, the tracking error ε undergoes oscillations around the stable tracking point. Since the discriminator is assumed to be linear around the zero crossing, the tracking error bias coincides with the position of the zero crossing of the discriminator function, as the oscillations are symmetric around the stable tracking point. In the presence of signal distortions, the discriminator function is distorted. The distorted discriminator functions for coherent and non-coherent DLLs are reported in Table 1, as a function of the cross-correlation (17). The parameter of the discriminator curve that determines the tracking error bias is the zero crossing. To graphically illustrate this point, in Fig. 3 we report a nominal discriminator function around the point $\varepsilon = 0$ and two distorted discriminator functions in the presence of constructive and destructive multipath. Multipath propagation can be seen as a particular case of analog distortion. In the case of having one multipath ray, the corresponding linear transfer function is

$$H(f) = \left[1 + \alpha_M e^{j2\pi f \tau_M}\right] \tag{18}$$

where α_M and τ_M are the complex attenuation constant and the time-delay of the multipath signal replica, respectively.

The initialization point of the tracking process is the result of the coarse synchronization process (acquisition). Let us indicate this initial value by ε_0. Let the set of all valid tracking points be denoted by $Z_{S(\varepsilon)}$ with $\varepsilon_{\text{lock}} \in Z_{S(\varepsilon)}$. The tracking error bias is the element of $Z_{S(\varepsilon)}$ closest to the initial point ε_0:

$$b_\varepsilon = \underset{\varepsilon_{\text{lock}} \in Z_{S(\varepsilon)}}{\operatorname{argmin}} \left|\varepsilon_{\text{lock}} - \varepsilon_0\right| \tag{19}$$

In the following results, we consider $\varepsilon_0 = 0$, i.e., the coarse synchronization is error-free. When expression (17) is substituted in the discriminators in Table 1, we get the analytic expression of the distorted discriminators in the frequency domain. For a coherent DLL, an error bias in the code tracking denoted as b_ε determines a bias b_φ in the estimation of the carrier phase φ. This is equal to the composite phase calculated at $\varepsilon = b_\varepsilon$:

$$b_\varphi = \vartheta_c\left(b_\varepsilon\right) \tag{20}$$

Tracking error jitter

The tracking error jitter for a coherent and a non-coherent tracking loop can be expressed as in (Holmes 2007, ch. 7):

$$\sigma_\varepsilon^2 = \begin{cases} \dfrac{2B_L N_T(0)}{P\left[S_c'\left(b_\varepsilon\right)\right]^2}, & \text{for coherent tracking loops} \\ \dfrac{2B_L N_T(0)}{P^2\left[S_c'\left(b_\varepsilon\right)\right]^2}, & \text{for non-coherent tracking loops} \end{cases} \tag{21}$$

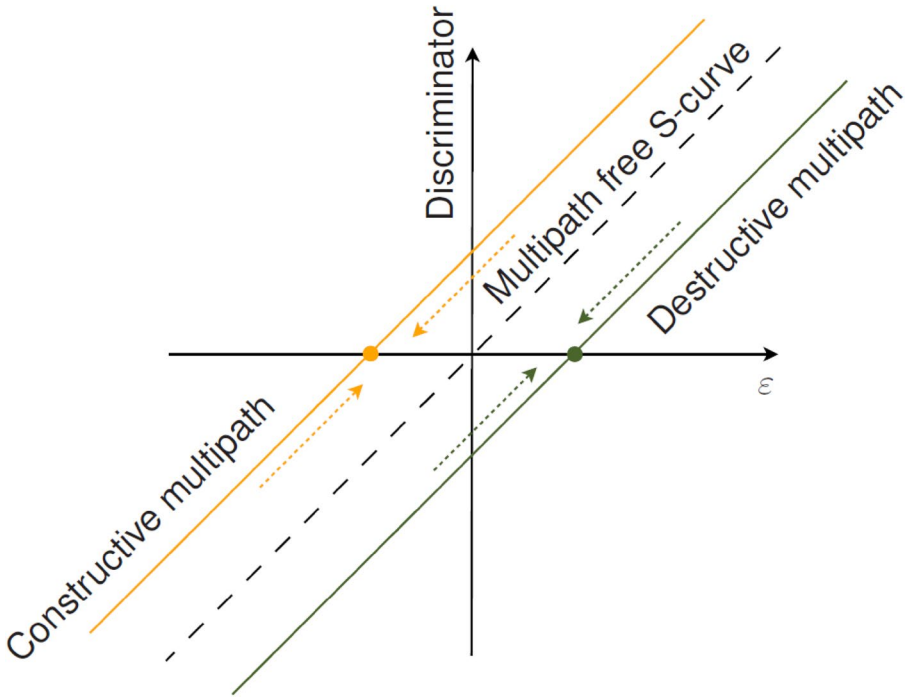

Fig. 3 Nominal discriminator and discriminator in the presence of multipath propagation

The quantity $N_T(f)$ is the PSD of the noise term of the error signal $n_T[k]$. The term $S_c'(b_\epsilon)$ indicates the derivative of the composite discriminator calculated at the tracking bias b_ϵ. B_L is the one-sided closed-loop noise bandwidth of the code-tracking loop, which is usually in the order of a few Hertz. Assuming that $N_T(f)$ is constant for $|f| \leq B_L$, then it can be approximated by $N_T(0)$. The noise term $n_T[k]$ and its PSD depend on the code-tracking loop structure, and therefore, the term $N_T(0)$ appearing in (22) does not represent the same quantity for coherent and non-coherent DLL. $n_T[k]$ is a function of the noise terms present at the output of the early and late correlators:

$$\begin{aligned} n_E[k] &= \frac{1}{T_p}\int_{\frac{k-1}{2}T_p}^{\frac{k+1}{2}T_p} n(t)\hat{c}(t+\Delta)\mathrm{d}t \\ n_L[k] &= \frac{1}{T_p}\int_{\frac{k-1}{2}T_p}^{\frac{k+1}{2}T_p} n(t)\hat{c}(t-\Delta)\mathrm{d}t \end{aligned} \tag{22}$$

These quantities are in general complex even when the nominal signal $c(t)$ is real. Real and imaginary parts will be indicated by a superscript I and Q, respectively. These noise terms are post-correlation noise, i.e., the discrete-time random process that is observable at correlator outputs when no input signal is present. The sampling time of this signal is the integration time, which in our case is T_p. Statistical characterization of the noise terms (22), which is necessary to characterize the noise term $n_T[k]$, can be obtained using the results developed for the analysis of the post-correlation noise, as in Proakis and Salehi (2008, p. 168), and the moments of Gaussian random processes (Krishnan 2006, p. 153; Davenport and Root 1958, p. 255; Papoulis 1991, p. 306).

In the following subsections, we report the expression of the PSD of the noise term $n_T[k]$ for a coherent early-minus-late and a non-coherent early-minus-late power DLL.

PSD of $n_T[k]$ in a coherent DLL

For the coherent early-minus-late DLL, the error term $n_T[k]$ present in the error signal $e[k]$ amounts to

$$n_T[k] = \frac{1}{T_p}\int_{\frac{k-1}{2}T_p}^{\frac{k+1}{2}T_p} n(t)[\hat{c}(t-\Delta) - \hat{c}(t+\Delta)]\mathrm{d}t = n_E^I[k] - n_L^I[k] \tag{23}$$

The autocorrelation of the noise term $n_T[k]$ is

$$R_{n_T}[x] = \frac{N_0}{T_p}\delta[x]\left[1 - R_{\hat{c}\hat{c}}(2\Delta)\right] \tag{24}$$

and moreover, its PSD is obtained as

$$N_T(f) = N_0\left[1 - R_{\hat{c}\hat{c}}(2\Delta)\right], \quad \text{for } -\tfrac{1}{2T_p} < f < \tfrac{1}{2T_p} \tag{25}$$

This PSD is constant and thus $N_T(f) = N_T(0)$.

PSD of $n_T[k]$ in a non-coherent DLL

In the non-coherent DLL, early-minus-late power, the noise term $n_T[k]$ of the error signal also contains cross-products:

$$\begin{aligned} n_T[k] = &\underbrace{2\sqrt{P}\left(R_{s\hat{c}}^I(\varepsilon-\Delta)n_L^I[k] - R_{s\hat{c}}^I(\varepsilon+\Delta)n_E^I[k]\right)}_{n_1^I[k]} \\ &+ \underbrace{\left|n_L^I[k]\right|^2 - \left|n_E^I[k]\right|^2}_{n_2^I[k]} \\ &\underbrace{+2\sqrt{P}\left(R_{s\hat{c}}^Q(\varepsilon-\Delta)n_L^Q[k] - R_{s\hat{c}}^Q(\varepsilon+\Delta)n_E^Q[k]\right)}_{n_1^Q[k]} \\ &+ \underbrace{\left|n_L^Q[k]\right|^2 - \left|n_E^Q[k]\right|^2}_{n_2^Q[k]} \end{aligned} \tag{26}$$

Its autocorrelation can be obtained using the formulas for the statistical characterization of the output of a square-law device (Davenport and Root 1958, p. 255):

$$R_{n_T}[x] = 4P\frac{N_0}{2T_p}\delta[x]\left[\rho_\Delta^I(b) + \rho_\Delta^Q(b)\right] + 2\frac{N_0^2}{T_p^2}\delta[x]\left(1 - R_{\hat{c}\hat{c}}^2(2\Delta)\right) \tag{27}$$

with

$$\begin{aligned} \rho_\Delta^I(\varepsilon) = &\left[R_{s\hat{c}}^I(\varepsilon-\Delta)\right]^2 + \left[R_{s\hat{c}}^I(\varepsilon+\Delta)\right]^2 \\ &- 2\left[R_{s\hat{c}}^I(\varepsilon-\Delta)R_{s\hat{c}}^I(\varepsilon+\Delta)\right]R_{\hat{c}\hat{c}}(2\Delta) \end{aligned} \tag{28}$$

$$\begin{aligned} \rho_\Delta^Q(\varepsilon) = &\left[R_{s\hat{c}}^Q(\varepsilon-\Delta)\right]^2 + \left[R_{s\hat{c}}^Q(\varepsilon+\Delta)\right]^2 \\ &- 2\left[R_{s\hat{c}}^Q(\varepsilon-\Delta)R_{s\hat{c}}^Q(\varepsilon+\Delta)\right]R_{\hat{c}\hat{c}}(2\Delta) \end{aligned} \tag{29}$$

resulting in

$$N_T(f) = PN_0\left(2\rho_\Delta^I(b) + 2\rho_\Delta^Q(b)\right) + \frac{N_0^2}{T_p}\left(2 - 2R_{\hat{c}\hat{c}}(2\Delta)\right) \tag{30}$$

The spectral noise densities (25) and (30) are then substituted in equation (21), and thus, we get an expression for the tracking error variance. Note that this expression also includes the effect of the pulse shape.

Study case: ICAO threat model A with arbitrary linear distortion

In the following, we study a generalization of the ICAO threat model C as an example of the application of the proposed model. Contrary to the ICAO threat model C, which encompasses threat model A and threat model B, and thus a second-order linear filtering is assumed, in this example, we consider threat model A followed by an arbitrary analog distortion, i.e., without restriction to a second-order step-response model as proposed in ICAO (2001).

The reason for this choice as an example is to offer further insight into the GNSS SQM discussion. To our best knowledge, the literature provides no accurate model for the joint occurrence of arbitrary analog and digital distortions and their implications on the pseudorange estimation. An arbitrary analog distortion is considered, as it has been shown that a second-order system, i.e., ICAO threat model B, is not always appropriate for modeling all GNSS signals (Phelts et al. 2009).

As test signals, we consider two DS-CDMA signals with two different chip pulse shapes: rectangular chip pulse shape or binary shift keying (BPSK) pulse and BOC(1,1) chip pulse shape. For each signal, we calculate the bias and the variance of the tracking error according to (19) and (21), for a one-sided bandwidth of $B = -12$ MHz. For the BPSK signal, the correlator spacings Δ/T_c span the interval between 0.05 and 0.5 chips; while for the BOC(1,1) signal the correlator spacings Δ/T_c span the interval between 0.05 and 0.25 chips. All correlator spacings refer to the half of the early–late spacing. The chip rate of both test signals is the same, $B_c = 1.023$ MHz. The value of the digital distortion has been chosen to be equal for both signals so that it can be observed how the same distortion impacts two different signals. As an analog distortion, we have considered a realistic but arbitrary transfer function as it will be described next. The theoretical results are validated with computer simulations using DLR software GNSS receiver.

Example of nonlinear distortion: digital distortion (ICAO threat model A)

The digital distortion for a non-band-limited signal causes flat tops or plateaus atop its cross-correlation peak (Phelts and Akos 2006) with an undistorted replica, and so a unique maximum point of the cross-correlation function cannot be determined. As a consequence of that, the discriminator curve is distorted and it does not cross the zero at only one point but it is identically zero within a range of values of the tracking error. Strictly speaking, such a signal is not trackable, as no stable tracking point exists, i.e., no unique absolute maximum exists for the cross-correlation function. This is due to the fact that the signal is not band-limited. Nevertheless, when the digital distortion is cascaded with an analog distortion, i.e., linear filtering, and in particular when the bandwidth of the analog filter is limited, the cross-correlation function has a unique maximum, and unambiguous tracking is possible. In the following, we shall indicate the generic ideal signal component by $s(t)$ and its digitally distorted counterpart by $s_\eta(t)$. The digital distortion is constant and it is quantified by the variable η, which expresses the delay of the falling edge in terms of the symbol time T_c.

In order to apply our performance assessment model, we need a mathematical expression for the PSD of the nonlinear distorted signal, i.e., $\boldsymbol{\Phi}_{TT}(f)$ as defined in (14), and the Fourier representation of the cross-correlation between the nonlinear distorted signal and the nominal signal used as a local replica in the receiver. This latter quantity is the CPS that we indicated by $\boldsymbol{\Psi}_{T\hat{c}}(f)$ in (13).

The PSD of a digitally distorted signal was already calculated by Bishop et al. (1998), though using different terminology, namely that of determining the PSD of a binary signal in the presence of data asymmetry. The PSD of a digitally distorted signal can be calculated as a particular case of the PSD of a generalized M-ary Markov data source that produces a random pulse train of M signals (Simon et al. 1995, p. 63):

$$\boldsymbol{\Phi}_{TT}(f) = \psi_c(f) + \psi_d(f) \tag{31}$$

where $\psi_c(f)$ and $\psi_d(f)$ are the frequency-continuous and the frequency-discrete components of the PSD, with

$$\psi_c(f)\frac{1}{T_c}\sum_{i=1}^{3} p_i\left|S_i'(f)\right|^2 + \frac{2}{T_c}\mathrm{Re}\left\{\sum_{i=1}^{3}\sum_{k=1}^{3} p_i S_i'^{*}(f) S_k'(f) p_{ik}\left(e^{-2j\pi fT}\right)\right\} \tag{32}$$

$$\psi_d(f) = \frac{1}{T_c^2}\sum_{n=-\infty}^{\infty}\left|\sum_{i=1}^{3} p_i S_i\left(\frac{n}{T_c}\right)\right|^2 \delta\left(f - \frac{n}{T_c}\right) \tag{33}$$

where $p_{i,k}\left(e^{-2j\pi fT}\right)$ indicates the Z-transform of the element i,k of the transition matrix as calculated in Bishop et al. (1998); $S_i(f)$ and p_i, with $i = 1, 2, 3$, are the three elementary signals in frequency domain and their respective probabilities. $S_i'(f)$, $i = 1, 2, 3$, represent the Fourier transforms of the elementary signals after the subtraction of their expected Fourier transforms:

$$S_i'(f) = S_i(f) - \sum_{k=1}^{3} p_k S_k(f) \tag{34}$$

In Simon et al. (1995, Section 3), one can find the definitions of the three elementary signals for the case of BPSK

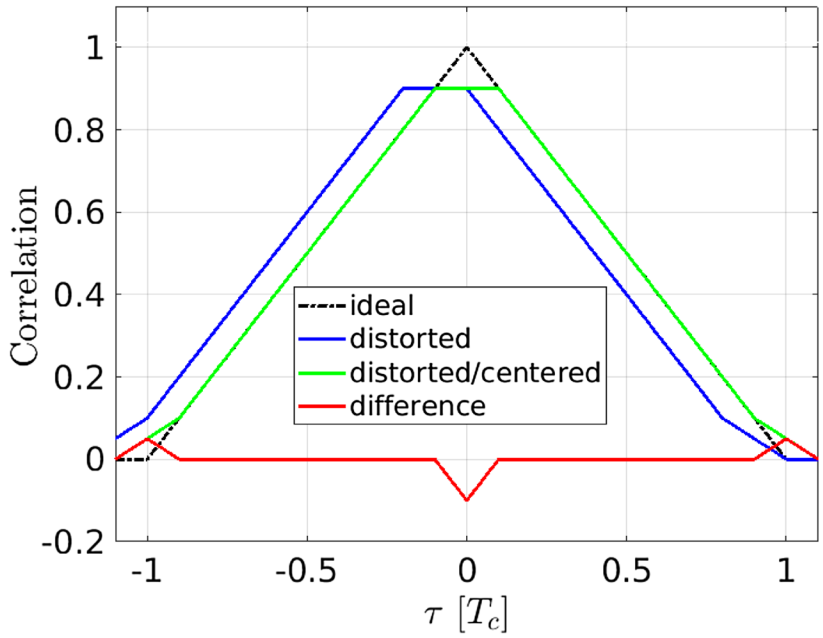

Fig. 4 Ideal and distorted correlation of a DS-CDMA ranging signal with a rectangular pulse shape and $\eta = 0.2$. Note that digital distortion also introduces a shift

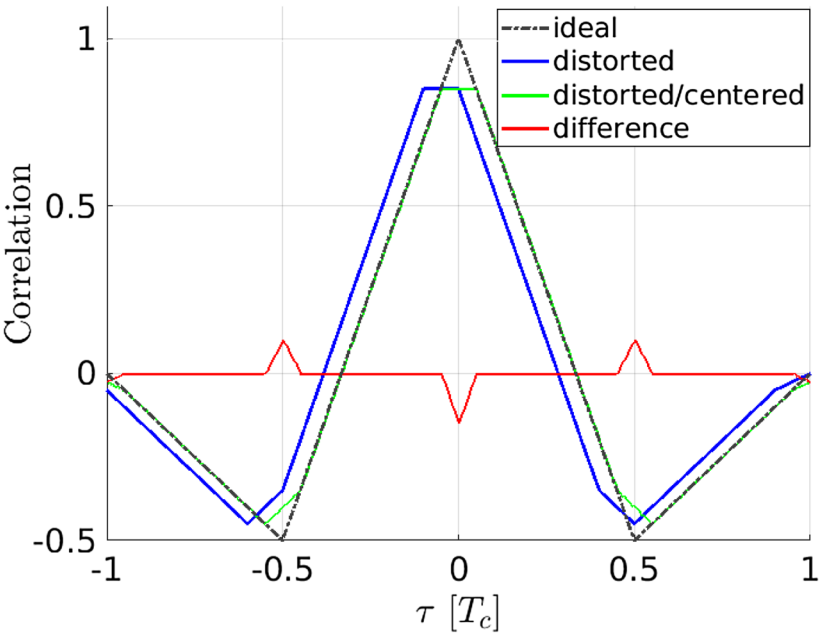

Fig. 5 Ideal and distorted correlation of a DS-CDMA ranging signal with a BOC(1,1) pulse shape and $\eta = 0.2$. Note that digital distortion also introduces a shift

and BOC(1,1) modulation, the latter under the name of "unbalanced asymmetric biphase modulation."

The shape of the main lobe of the cross-correlation function (CCF) (11) between a digitally distorted DS-CDMA signal and its ideal (non-distorted) version can be parameterized by the digital distortion η. The variable η can be both positive and negative, and thus, it can model either an advance or a delay of the falling edge. In Fig. 4, the main lobe of the CCF is presented for the case of a DS-CDMA signal with a rectangular chip shape pulse. In Fig. 5, the same quantity is depicted for the case of a DS-CDMA signal with a BOC(1,1) or biphase chip shape pulse, for the same value of digital distortion.

The solid blue line in Figs. 4 and 5 shows the CCF when the local replica is correlated with a digitally distorted signal, where $\eta > 0$. Besides changing the shape of the original autocorrelation function (ACF), the digital distortion also causes a time shift, which is toward negative delays if $\eta > 0$ and toward positive delays if $\eta < 0$. We describe the distorted CCFs (blue line) in terms of a weighted sum of triangular functions (red line), and then, we calculate the CPSs as the Fourier transform of the CCFs. Note that the digital

distortion also introduced a time shift, and for this reason, in Figs. 4 and 5 we depict a "centered" distorted CCF (green line). For BPSK, the distorted CCF amounts to

$$\varphi_{BPSK}(\varepsilon) = R_{cc}^{BPSK}\left(\varepsilon + \eta T_c\right) + \frac{|\eta|}{4}\mathrm{tri}\left(\frac{\varepsilon + T_c(1+\eta)}{\frac{\eta T_c}{2}}\right) + \frac{|\eta|}{4}\mathrm{tri}\left(\frac{\varepsilon - T_c(1-\eta)}{\frac{\eta T_c}{2}}\right) - \frac{|\eta|}{2}\mathrm{tri}\left(\frac{\varepsilon + \eta T_c}{\frac{\eta T_c}{2}}\right) \tag{35}$$

where

$$\mathrm{tri}\left(\frac{\tau}{T}\right) = \begin{cases} 1 - \frac{|\tau|}{T}, & \text{for } |\tau| \le T \\ 0, & \text{else} \end{cases} \tag{36}$$

and $R_{cc}^{\mathrm{BPSK}}(\tau)$ is the ideal ACF (in particular the main lobe) of the nominal signal $c(t)$

$$R_{cc}^{\mathrm{BPSK}}(\tau) = \int_{-\infty}^{\infty} c(t)c(t+\tau)\mathrm{d}t = \mathrm{tri}\left(\frac{\tau}{T_c}\right) \tag{37}$$

The Fourier pair $\mathrm{tri}(\tau/T) \Leftrightarrow \mathrm{sinc}^2(\mathrm{fT})$ can be used to calculate the Fourier transform of (35), i.e., the CPS:

$$\Psi_{T\hat{c}}^{BPSK}(f) = \left(\Phi_{cc}^{BPSK}(f) - \frac{\eta^2 T_c}{4}\sin c^2\left(\frac{f\eta T_c}{2}\right)\left(1 - \cos\left(2\pi f T_c\right)\right)\right)e^{-j\pi f\eta T_c} \tag{38}$$

The CPS of a digitally distorted sine-phased BOC(n_s,1) can be calculated in a similar fashion:

$$\Psi_{T\hat{c}}^{\mathrm{BOC}(n_s,1)}(f) = \left(\Phi_{cc}^{BOC(n_s,1)}(f) + \Phi_{\eta}(f)\right)e^{-j\pi f\eta T_c} \tag{39}$$

with

$$\Phi_{cc}^{BOC(n_s,1)}(f) = T_c^2\left(\mathrm{sinc}\left(fT_c\right)\tan\left(\frac{\pi f T_c}{2n_S}\right)\right)^2 \tag{40}$$

and

$$\Phi_{\eta}(f) = \left(1 - 4n_s\right)\frac{\eta^2 T_c}{4}\mathrm{sinc}^2\left(\frac{f\eta T_c}{2}\right)\left[1 + \sum_{k=1}^{2n_s-1}(-1)^k\frac{2n_s - k}{n_s - 0.25}\cos\left(\pi f T_c\frac{k}{n_s}\right)\right] \tag{41}$$

One gets the expression for a sine-phased BOC(1,1) by substituting $n_s = 1$ in the above expressions.

Linear distortion (ICAO threat model B)

As a linear distortion, we consider a realistic transfer function. The transfer function we consider was observed in the E1 band of a Galileo satellite with the pseudorandom sequence (PRN) number 11. This transfer function is depicted in Fig. 6. Notice that the phase spectrum shows a mild slope. This corresponds to a minor delay in the signal introduced by the satellite hardware. In the calculation of the pseudorange, this delay is included in the clock error term and causes no impact on the receiver if and only if this delay due to hardware is the same for all satellites considered for positioning. In case each satellite introduces a different delay, this causes an error in the positioning.

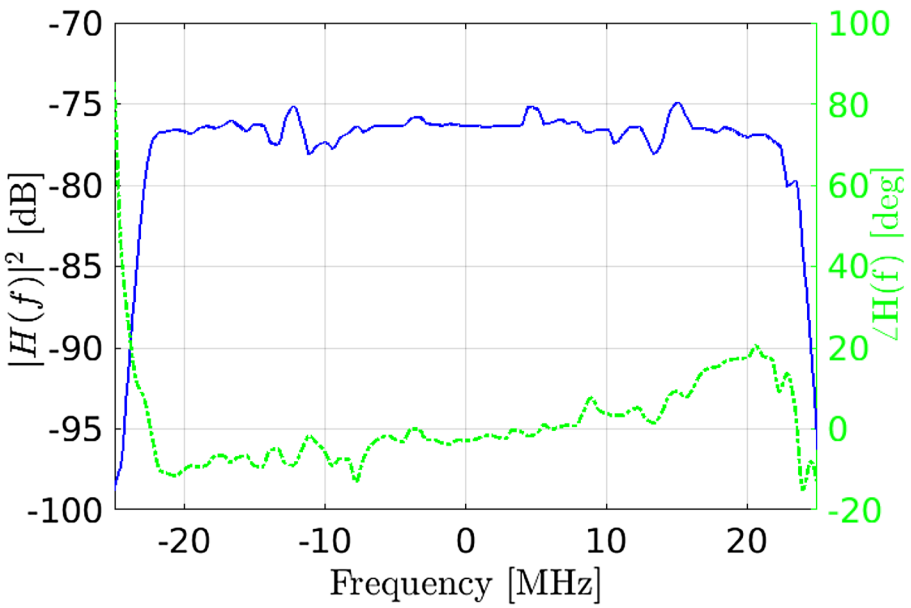

Fig. 6 Transfer function responsible for the linear distortion

Table 2 Parameters of the synthetic signal

Parameter	Value
η	0.05
Chip rate	1.023 MHz
C/N_0	50 dB-Hz
Duration	30 s
Resolution	8 bits

Table 3 Parameters of GNSS receiver

Parameter	Value
DLL type	Coherent
B (baseband)	12 MHz
T_p	2 ms
B_L	5 Hz

Assessment and verification

The validation of the theoretical results has been implemented as follows. Two synthetic signals have been generated with the parameters reported in Table 2. The two signals under test, a BPSK and a BOC(1,1), are used to drive a bit-true GNSS software receiver whose parameters are reported in Table 3. The bias of the tracking error obtained via software simulations is the difference between the true signal delay and the delay to which the software GNSS receiver converges. The tracking error jitter is the standard deviation of the tracking point around the resulting code phase bias. The resulting code phase tracking bias b_ϵ and the tracking jitter σ_ϵ for the BPSK signal are reported in Figs. 7 and 8, while the results related to the BOC(1,1) signal are depicted in Figs. 9 and 10. For both signals, the same distortions have been applied. The linear filtering is reported in Fig. 6, and the digital distortion has $\eta = 0.05$. The distortions seem to affect a bit more the bias of the BOC(1,1) signal than the BPSK signal. The mean value of the bias over the correlator spacing is given mostly by the value of the digital distortion, while the course of the curve is given mostly by the analog distortion. Our theoretical results are in perfect agreement with the simulated ones, thus confirming the validity of the model developed.

It is important to remark that the joint impact of threat model A and threat model B is sometimes constructive and other times destructive. As shown in Fig. 11, the pseudorange bias evaluated for $\eta = \mp 0.5\%$ is not the same in magnitude. This is due to the fact that for negative values of η threat model A partially compensates the effect of threat model B, while for positive values of η the effects of threat model A and threat model B add constructively.

Conclusions

We presented an analytic assessment of the GNSS receiver code-tracking performance in the presence of linear and nonlinear distortions. The main novelty of the research consists in proposing a method to assess GNSS receiver performance when both linear and nonlinear distortions are impairing the ranging signal. The proposed model was validated with a DLR GNSS software receiver.

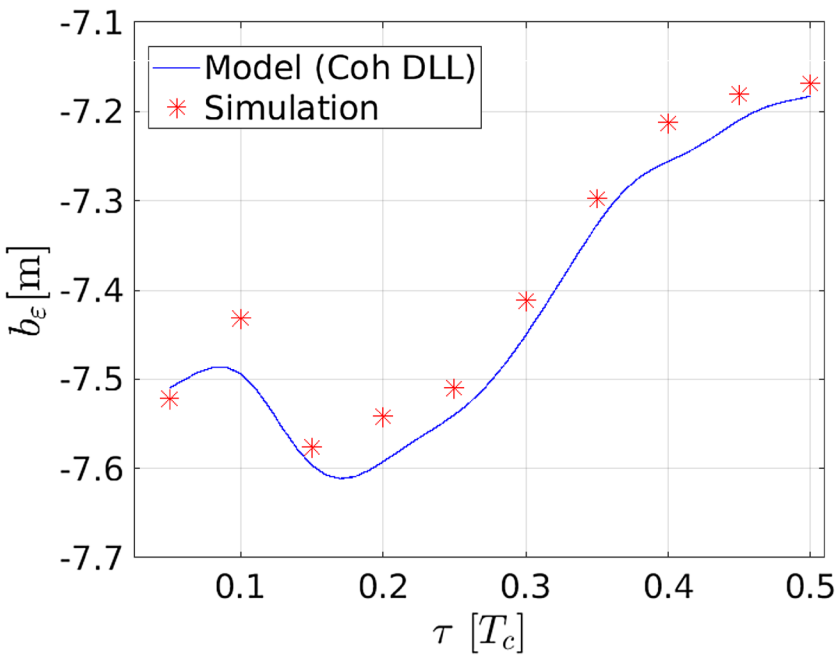

Fig. 7 Bias of the tracking error for a BPSK signal. The parameters are reported in Tables 2 and 3

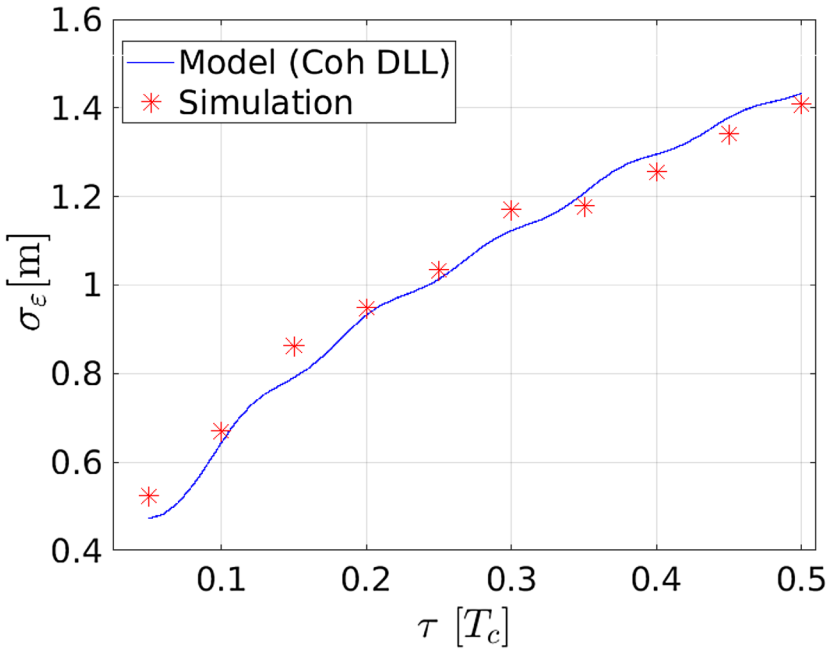

Fig. 8 Jitter of the tracking error for a BPSK signal. The parameters are reported in Tables 2 and 3

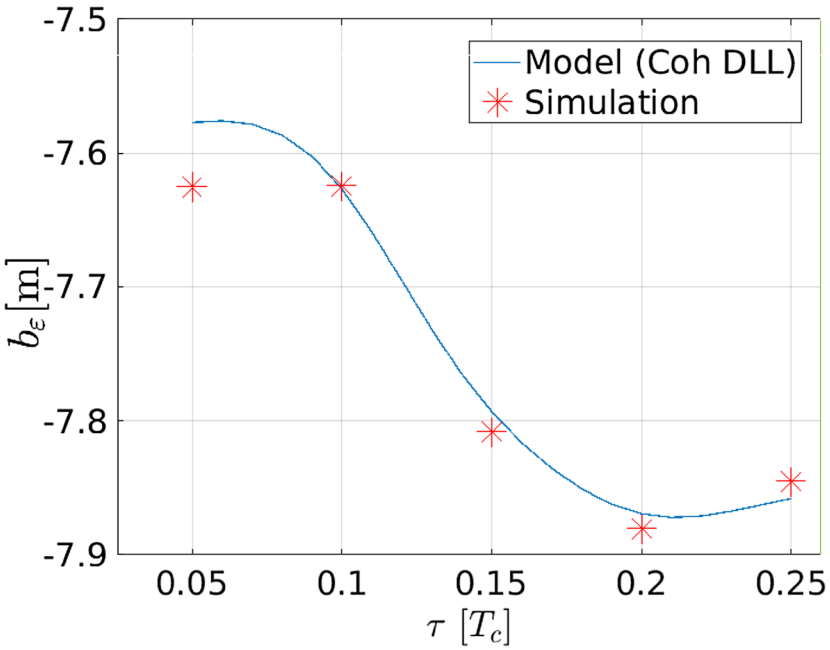

Fig. 9 Bias of the tracking error for a BOC(1,1) signal. The parameters are reported in Tables 2 and 3

The joint effect of linear and nonlinear distortions on the GNSS receiver performance is assessed by deriving analytical formulas for the tracking error bias and the tracking error variance. The linear and nonlinear distortions are parameters of these formulas. The proposed model is general enough to include an arbitrary nonlinear distortion, provided that a model of the CPS between the output of this nonlinear distortion and the local replica is available. In case of a lack of a mathematic model, empirical models for the CPS can be used. No assumption needs to be made on the linear distortion. The limitations of this work derive from the stationarity assumptions made both for the satellite distortions and for the user characterization. As a result of that, the impact of satellite distortions on the capability of the receiver to keep the lock on the signals is not part of this model.

This work finds direct application in the characterization of satellite payload distortions, avoiding complex signal-level simulations and providing a tool to distinguish nominal signal distortions from signal anomalies addressing

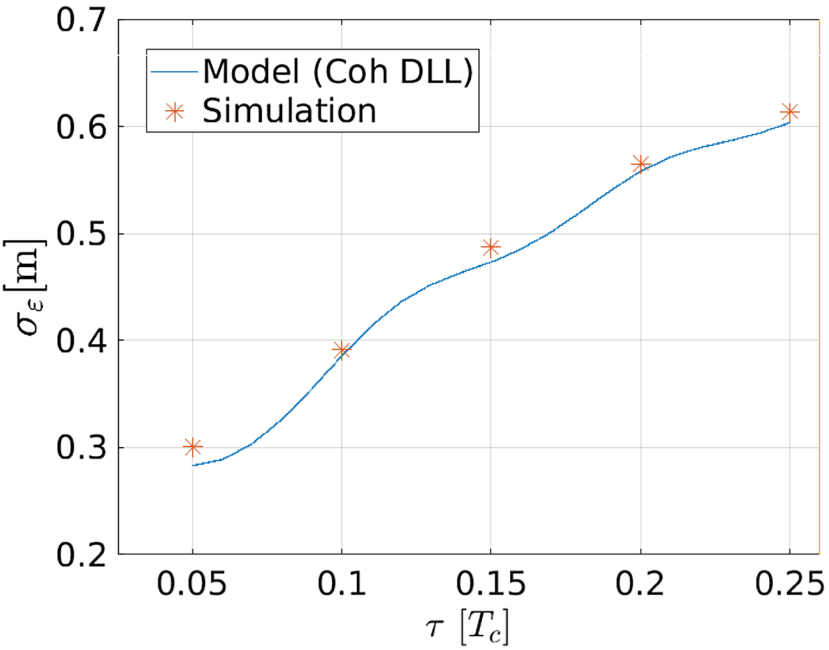

Fig. 10 Jitter of the tracking error for a BOC(1,1) signal. The parameters are reported in Tables 2 and 3

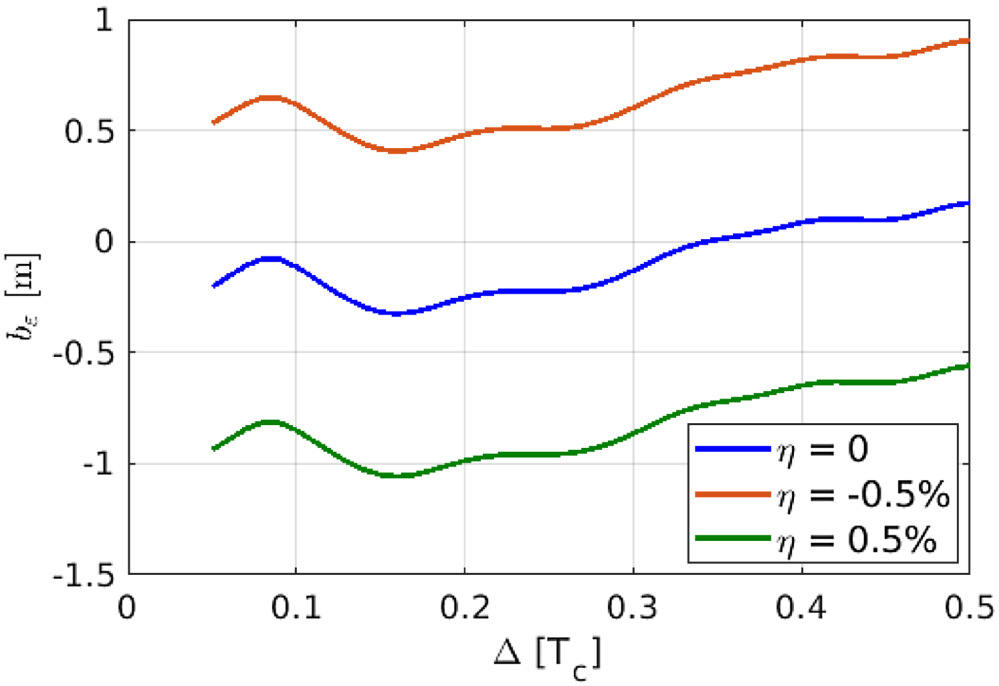

Fig. 11 Tracking error bias for BPSK signal for different values of η (threat model A)

user performance. Moreover, the accurate statistical characterization of the tracking error regarding bias and variance presented herein is very useful in producing more accurate estimates of the protection level risks and the corresponding probabilities of misleading information, see, e.g., Soualle et al. (2015), Zaugg(2002) and Van Dierendonck et al. (2000a, b). In particular, the proposed model provides an analytical formula for the tracking error variance, even though only with the ideal receiver front-end assumption. This constitutes a step toward the possibility of removing a common assumption made in the above-mentioned literature that considers the variance equal in both nominal and degraded modes. Indeed, removing this assumption could be justified in some cases, since signal distortions that cause a large increase in the variance of the tracking error cannot be ruled out. For example, this is the case when distortion causes the discriminator gain to decrease, i.e., when the CCF peak becomes less sharp. The main advantage of an accurate estimate for the bias and variance of the pseudorange error is that this enables making more efficient use of the allocated integrity risk, by complying with the integrity requirements with less margin.

Appendix: Discriminator gains

The discriminator gain is the derivative of the discriminator calculated at the tracking point, i.e., at the bias point.

Coherent DLL discriminator gain

The discriminator gain of a coherent DLL is:

$$\begin{aligned} S_c'(b_\varepsilon) = \frac{\partial S(\varepsilon)}{\partial \varepsilon}|_{\varepsilon=b_\varepsilon} &= 2\Bigg(\int_{-B}^{B} \Psi^{\mathrm{R}}_{\mathrm{even}}(f)(2\pi f)\cos\left(2\pi f b_\varepsilon\right)\sin\left(2\pi f\Delta\right)\mathrm{d}f \\ &\quad - \int_{-B}^{B} \Psi^{\mathrm{I}}_{\mathrm{odd}}(f)(2\pi f)\sin\left(2\pi f b_\varepsilon\right)\sin\left(2\pi f\Delta\right)\mathrm{d}f\Bigg)\cos\left(\vartheta\left(b_\varepsilon\right)\right) \\ &\quad - 2\Bigg(\int_{-B}^{B} \Psi^{\mathrm{R}}_{\mathrm{even}}(f)(2\pi f)\sin\left(2\pi f b_\varepsilon\right)\sin\left(2\pi f\Delta\right)\mathrm{d}f \\ &\quad - \int_{-B}^{B} \Psi^{\mathrm{I}}_{\mathrm{odd}}(f)(2\pi f)\cos\left(2\pi f b_\varepsilon\right)\sin\left(2\pi f\Delta\right)\mathrm{d}f\Bigg)\sin\left(\vartheta\left(b_\varepsilon\right)\right)\vartheta'\left(b_\varepsilon\right) \\ &\quad + 2\Bigg(\int_{-B}^{B} \Psi^{\mathrm{I}}_{\mathrm{even}}(f)(2\pi f)\cos\left(2\pi f b_\varepsilon\right)\sin\left(2\pi f\Delta\right)\mathrm{d}f \\ &\quad + \int_{-B}^{B} \Psi^{\mathrm{R}}_{\mathrm{odd}}(f)(2\pi f)\cos\left(2\pi f b_\varepsilon\right)\sin\left(2\pi f\Delta\right)\mathrm{d}f\Bigg)\sin\left(\vartheta\left(b_\varepsilon\right)\right) \\ &\quad + 2\Bigg(\int_{-B}^{B} \Psi^{\mathrm{I}}_{\mathrm{even}}(f)(2\pi f)\sin\left(2\pi f b_\varepsilon\right)\sin\left(2\pi f\Delta\right)\mathrm{d}f \\ &\quad - \int_{-B}^{B} \Psi^{\mathrm{R}}_{\mathrm{odd}}(f)(f)(2\pi f)\cos\left(2\pi f b_\varepsilon\right)\sin\left(2\pi f\Delta\right)\mathrm{d}f\Bigg)\cos\left(\vartheta\left(b_\varepsilon\right)\right)\vartheta'\left(b_\varepsilon\right) \end{aligned} \tag{42}$$

When there is a real and even cross-power spectral density, e.g., in the absence of distortion and with the local replica equal to the transmitted signal, the above formula collapses to

$$S_c'(0) = 2\int_{-B}^{B} \Psi(f)(2\pi f)\sin\left(2\pi f\Delta\right)\mathrm{d}f \tag{43}$$

with $\vartheta_c'\left(b_\varepsilon\right)$ being the derivative of the composite phase calculated at the bias point b_ε.

Introducing the following definition

$$\xi(\varepsilon) = \frac{R^{Q}_{s\hat{c}}(\varepsilon)}{R^{I}_{s\hat{c}}(\varepsilon)} = \frac{\int_{-B}^{B}\Psi^{\mathrm{R}}_{\mathrm{odd}}(f)\sin(2\pi f\varepsilon)\mathrm{d}f + \int_{-B}^{B}\Psi^{\mathrm{I}}_{\mathrm{even}}(f)\cos(2\pi f\varepsilon)\mathrm{d}f}{\int_{-B}^{B}\Psi^{\mathrm{R}}_{\mathrm{even}}(f)\cos(2\pi f\varepsilon)\mathrm{d}f - \int_{-B}^{B}\Psi^{\mathrm{I}}_{\mathrm{odd}}(f)\sin(2\pi f\varepsilon)\mathrm{d}f} \tag{44}$$

then we can write

$$\vartheta_c(\varepsilon) = \arctan(\xi(\varepsilon)) \tag{45}$$

$$\vartheta_c'(\varepsilon) = \frac{1}{1+\xi^2(\varepsilon)}\xi'(\varepsilon) \tag{46}$$

which defines the composite phase term.

Non-coherent DLL discriminator gain

The discriminator gain of a non-coherent DLL is

$$
\begin{aligned}
S'\left(b_\varepsilon\right) = 2\Bigg[&\int_{-B}^{B} \Psi^{\mathrm{R}}_{\mathrm{even}}(f)\cos\left(2\pi f\left(b_\varepsilon-\Delta\right)\right)\mathrm{d}f \\
&-\int_{-B}^{B} \Psi^{\mathrm{I}}_{\mathrm{odd}}(f)\sin\left(2\pi f\left(b_\varepsilon-\Delta\right)\right)\mathrm{d}f\Bigg]\cdot \\
&\Bigg[-\int_{-B}^{B} \Psi^{\mathrm{R}}_{\mathrm{even}}(f)(2\pi f)\sin\left(2\pi f\left(b_\varepsilon-\Delta\right)\right)\mathrm{d}f \\
&-\int_{-B}^{B} \Psi^{\mathrm{I}}_{\mathrm{odd}}(f)(2\pi f)\cos\left(2\pi f\left(b_\varepsilon-\Delta\right)\right)\mathrm{d}f\Bigg] \\
&+2\Bigg[\int_{-B}^{B} \Psi^{\mathrm{R}}_{\mathrm{odd}}(f)\sin\left(2\pi f\left(b_\varepsilon-\Delta\right)\right)\mathrm{d}f \\
&+\int_{-B}^{B} \Psi^{\mathrm{I}}_{\mathrm{even}}(f)\cos\left(2\pi f\left(b_\varepsilon-\Delta\right)\right)\mathrm{d}f\Bigg]\cdot \\
&\Bigg[\int_{-B}^{B} \Psi^{\mathrm{R}}_{\mathrm{odd}}(f)(2\pi f)\cos\left(2\pi f\left(b_\varepsilon-\Delta\right)\right)\mathrm{d}f \\
&-\int_{-B}^{B} \Psi^{\mathrm{I}}_{\mathrm{even}}(f)(2\pi f)\sin\left(2\pi f\left(b_\varepsilon-\Delta\right)\right)\mathrm{d}f\Bigg] \\
&-2\Bigg[\int_{-B}^{B} \Psi^{\mathrm{R}}_{\mathrm{even}}(f)\cos\left(2\pi f\left(b_\varepsilon+\Delta\right)\right)\mathrm{d}f \\
&-\int_{-B}^{B} \Psi^{\mathrm{I}}_{\mathrm{odd}}(f)\sin\left(2\pi f\left(b_\varepsilon+\Delta\right)\right)\mathrm{d}f\Bigg]\cdot \\
&\Bigg[-\int_{-B}^{B} \Psi^{\mathrm{R}}_{\mathrm{even}}(f)(2\pi f)\sin\left(2\pi f\left(b_\varepsilon+\Delta\right)\right)\mathrm{d}f \\
&-\int_{-B}^{B} \Psi^{\mathrm{I}}_{\mathrm{odd}}(f)(2\pi f)\cos\left(2\pi f\left(b_\varepsilon+\Delta\right)\right)\mathrm{d}f\Bigg] \\
&-2\Bigg[\int_{-B}^{B} \Psi^{\mathrm{R}}_{\mathrm{odd}}(f)\sin\left(2\pi f\left(b_\varepsilon+\Delta\right)\right)\mathrm{d}f \\
&+\int_{-B}^{B} \Psi^{\mathrm{I}}_{\mathrm{even}}(f)\cos\left(2\pi f\left(b_\varepsilon+\Delta\right)\right)\mathrm{d}f\Bigg]\cdot \\
&\Bigg[\int_{-B}^{B} \Psi^{\mathrm{R}}_{\mathrm{odd}}(f)(2\pi f)\cos\left(2\pi f\left(b_\varepsilon+\Delta\right)\right)\mathrm{d}f \\
&-\int_{-B}^{B} \Psi^{\mathrm{I}}_{\mathrm{even}}(f)(2\pi f)\sin\left(2\pi f\left(b_\varepsilon+\Delta\right)\right)\mathrm{d}f\Bigg]
\end{aligned}
\tag{47}
$$

When there is a real and even CPS, e.g., in the absence of distortion, and local the replica is matched to the received signal, the above formula form collapses to

$$
S'_c(0) = 4\int_{-B}^{B} \Psi(f)\cos\left(2\pi f\Delta\right)\mathrm{d}f \int_{-B}^{B} \Psi(f)\sin\left(2\pi f\Delta\right)\mathrm{d}f \tag{48}
$$

which is the same formula as in Holmes (2007).

References

Akos D, Phelts RE, Pullen S, Enge P (2000) Signal quality monitoring: test results. In: Proceedings of ION NTM 2000, Institute of Navigation, Anaheim, CA, 26–28 January 2000, pp 536–541

Betz JW, Kolodziejski KR (2009) Generalized theory of code tracking with an early-late discriminator part I: lower bound and coherent processing. IEEE Trans Aerosp Electron Syst 45:1538–1550

Bishop DF, Million S, Nguyen TM, Simon MK (1998) The power spectrum of unbalanced NRZ and biphase signals in the presence of data asymmetry. IEEE Trans Electromagn Compat 40:55–62

Braasch MS (1992) On the characterization of multipath errors in satellite based precision approach and landing systems. Dissertation Ohio University

Davenport WB, Root WL (1958) An introduction to the theory of random signals and noise. McGraw-Hill, Inc, New York

Hegarty CJ, Van Dierendonck AJ (2008) Recommendations on digital distortion requirements for the civil GPS signals. In: Position, Location and Navigation Symposium, IEEE/ION 2008

Holmes JK (1997) Noncoherent late minus early power code tracking performance with front end filtering. In: Proceedings of ION GPS 1997, Institute of Navigation, Kansas City, USA, 16–19 September 1997, pp 583–591

Holmes JK (2007) Spread spectrum systems for GNSS and wireless communications. Artech House, Inc., Norwood

ICAO (2001) International Standards and Recommended Practices, Annex 10, Attachment D

Irsigler M (2008) Multipath propagation, mitigation and monitoring in the light of Galileo and modernized GPS. Dissertation, Bundeswehr University, Munich

Kay SM (1998) Fundamentals of statistical signal processing, volume I: estimation theory. Prentice Hall, Inc., Upper Saddle River

Krishnan V (2006) Probability and random processes. Wiley, Hoboken

Mittelman AM, Phelts E, Akos D, Pullen S, Enge P (2004) Signal deformations on nominally healthy GPS satellites. In: Proceedings of ION NTM 2004, Institute of Navigations, San Diego, USA, 26–28 January 2004

Pagot J-B, Thevenon P, Julien O (2016) Signal quality monitoring for new GNSS signals. Dissertation, ENAC, Toulouse

Papoulis A (1991) Probability, random variables and stochastic processes, 3rd edn. McGraw-Hill, Inc., New York

Phelts RE (2001) Multicorrelator techniques for robust mitigation of threats to GPS signal quality. Dissertation, Stanford University

Phelts RE, Akos DM (2006) Effects of signal deformations on modernized GNSS signals. J Glob Position Syst 5:2–10

Phelts RE, Walter T, Enge P (2009) Characterizing nominal analog signal deformation on GNSS signals. In: Proceedings of ION GNSS 2009, Institute of Navigation, Savannah, USA, 22–25 September 2009, pp 1343–1350

Proakis JG, Salehi M (2008) Digital communications, 5th edn. McGraw Hill, Inc., New York

Simon MK, Million S (1996) The power spectrum of unbalanced NRZ and biphase signals in the presence of data asymmetry. Technical Report, Jet Propulsion Laboratory, California Institute of Technology, USA

Simon MK, Hinedi SM, Lindsey WC (1995) Digital communications techniques. McGraw Hill, Inc., New York

Soellner M, Kohl R, Luetke W, Erhard P (2002) The impact of linear and non-linear signal distortions on Galileo code tracking accuracy. In: Proceedings of ION GPS, Institute of Navigation, Portland, Oregon, 24–27 September 2002, pp 1270–1285

Soualle F, Mink M, Braun R, Carcanague S, Boyer M (2015) Methodology for the design of integrity barriers in a regional augmentation satellite system. In: Proceedings of ION GNSS + 2015, Institute of navigation, Tampa, USA, 14–18 September 2015, pp 1551–1564

Van Dierendonck AJ, Akos D, Pullen S, Enge P (2000) Practical implementation considerations in the detection of GPS satellite failure. In: Proceedings of IAIN World Congress 56th Annual Meeting of the Institute of Navigation, San Diego, USA, 26–28 June 2000

Van Dierendonck AJ, Akos D, Pullen S, Phelts RE, Enge P (2000). Practical implementation considerations in the detection of GPS satellite signal failure. In: Proceedings of IAIN World Congress and ION AM, Institute of Navigation, San Diego, CA, 26–28 June 2000

Van Nee DJR (1995) Multipath and multi-transmitter Interference in Spread-Spectrum communication and Navigation systems. Dissertation, Technical University of Delft

Vergara M, Antreich F, Meurer M (2009) Effect of multipath on code-tracking error jitter of a delay locked loop. In: Proceedings of 4th European Workshop on GNSS Signals and Signal Processing, GNSS Signal 2009, Wessling, Germany

Vergara M, Sgammini M, Thoelert S, Enneking C, Zhu Y, Antreich F (2016) Tracking error modeling in presence of satellite imperfections. Navigation 63(1):3–13

Wong G, Phelts ER, Walter T, Enge P (2011) Alternative characterization of analog signal deformation for GNSS-GPS satellites. In: Proceedings of ION ITM 2011, Institute of Navigation, San, Diego, 24–26 January 2011, pp 497–507

Wu X, Ling C, Xiang H (2002) Despreading chip waveform design for coherent delay-locked tracking in DS–SS systems. In: IEEE International Conference on Communications, ICC 2002, New York, USA, April 28–May 2, pp 631–635

Zaugg T (2002) A new evaluation of maximum allowable errors and missed detection probabilities for LAAS ranging source monitors. In: Proceedings of ION AM 2002, Institute of Navigation and CIGTF 21st Guidance Test Symposium, Albuquerque, NM, 24–26 June 2002, pp 187–194

Mariano Vergara received the B.Sc. and M.Sc. degrees in Telecommunications Engineering from the University of Naples Federico II, Italy, in 2006, and from the Technische Universität Kaiserslautern (TU-KL), Germany, in 2009, respectively. For 7 years, he was an associate researcher at Institute of Communications and Navigation of the German Aerospace Center (DLR), Wessling-Oberpfaffenhofen. He is a Ph.D. candidate at Universitat Autònoma de Barcelona. In 2017, he was a visiting scientist in the Department of Teleinformatics Engineering (DETI) at the Federal University of Ceará (UFC) in Fortaleza, Brazil. He joined Airbus Defense and Space in 2018.

Felix Antreich received the diploma degree in Electrical Engineering from the Munich University of Technology (TUM), Munich, Germany, in 2003. In 2011, he also received the Doktoringenieur (Ph.D.) degree from the TUM. From September 2016 to early 2018, he was a visiting professor in the Department of Teleinformatics Engineering (DETI) at the Federal University of Ceará (UFC) in Fortaleza, Brazil. He is currently an associate professor at the Aeronautics Institute of Technology (ITA) in São José do Campo, Brazil.

Christoph Enneking received the B.Sc. and M.Sc. degrees in Electrical Engineering from the Munich University of Technology (TUM), Germany, in 2012 and 2014, respectively. In September 2014, he joined the Institute of Communications and Navigation of the German Aerospace Center (DLR), Wessling-Oberpfaffenhofen. His research interests include GNSS signal design, estimation theory and GNSS intra- and intersystem interference.

Matteo Sgammini received the M.Eng. degree in Electrical Engineering in 2005 from the University of Perugia. He joined the Institute of Communications and Navigation of DLR in 2008. He is currently pursuing a Ph.D. in Electrical Engineering with research interests in interference mitigation techniques for GNSS. Current research activity includes adaptive filtering, array signal processing and estimation theory for GNSS.

Prof. Gonzalo Seco-Granados received the Ph.D. degree in Telecommunications Engineering from the Universitat Politècnica de Catalunya, in 2000, and the MBA degree from IESE Business School, in 2002. Until 2005, he was with the European Space Agency, involved in the design of the Galileo System. Since 2006, he has been an associate professor in the Department of Telecommunications, Universitat Autònoma de Barcelona.